Journal of Physical Oceanography

The DOI for this manuscript is doi: 10.1175/JPO-D-17-0054.1

The final published version of this manuscript will replace the preliminary version at the above DOI once it is available.

If you would like to cite this EOR in a separate work, please use the following full citation:

MacMahan, J., 2017: Increased aerodynamic roughness owing to surfzone foam. J. Phys. Oceanogr. doi:10.1175/JPO-D-17-0054.1, in press.

Increased aerodynamic roughness owing to surfzone foam

Jamie MacMahan[1]

[1]Oceanography Department, Naval Postgraduate School, Monterey, CA 93933; 831-656-2379; jhmacmah@nps.edu

Abstract: Drag coefficients (C_d) obtained through direct eddy-covariance estimates of the wind stress were observed at four different sandy beaches with dissipative surf zones along the coastline of Monterey Bay, CA, USA. The measured surfzone C_d (~$2x10^{-3}$) is twice as large as open ocean estimates and consistent with recent estimates of C_d over the surf zone and shoaling region. Owing to the heterogeneous nature of the nearshore consisting of non-breaking shoaling waves and breaking surfzone waves, the surfzone wind stress source region is estimated from the footprint probability distribution derived for stable and unstable atmospheric conditions. An empirical model developed for estimating the C_d for open ocean foam coverage dependent on wind speed, is modified for foam coverage owing to depth-limited wave breaking within the surf zone. A modified empirical C_d model for surf zone foam predicts similar values as the measured C_d and provides an alternative mechanism to describe roughness.

1. Introduction

Over land, the geometric surface roughness (*k*) and corresponding aerodynamic roughness (z_o) for surface features can be considered temporally constant. Over the open ocean, z_o is a function of both surface texture (associated viscous surface stresses) and the local wave field (associated form drag and flow separation). The associated stresses are dynamically coupled with the wind, can evolve together, and transition from viscous stresses to wave stresses. Non-local wave fields further complicate the dynamical relationship. Numerous, extensive, *open-ocean* field studies have investigated the various stress relationships, resulting in both consistencies and discrepancies (see Edson et al., 2013 for an overview).

Until recently, there have been limited observations of the air-ocean momentum fluxes in the *nearshore* region of the ocean. The nearshore region includes the surface gravity wave shoaling region (~< 30m depth) and the dissipative surf zone (~< 2m depth). Unlike the open ocean, surface gravity waves become decoupled from the wind-wave relationship and dependent on water depth (h), modifying the dynamical-coupling between the wind and the waves. Furthermore, depth-limited wave breaking occurs within the surf zone reducing the wave height.

Hsu (1970) and Vugts and Cannemeijer (1981) measured elevated drag coefficients, $C_d \sim O(1x10^{-3} – 5x10^{-3})$, related to the surf zone and swash zone. Smith and Bank (1975) recognized that depth-limited wave breaking may have increased their measured C_d owing to their tower being deployed on a sand spit. During Hurricane Ike in 2008, Zachary et al. (2013) and Powell (2008) measured elevated C_d values in the nearshore compared with the open ocean. Anctil and Donelan (1996) found increased C_d values for waves shoaling from

12 m to breaking in 2 m water depth. Shabani et al. (2014, 2016) found that measured C_d for near-neutral, atmospheric stability over the shoaling region and surf zone were O(2) times larger than open-ocean estimates, which they ascribe to the wave celerity (c) and shape effects. Similar to Anctil and Donelan (1996), they suggested that as the wave shoals, wave speed slows relative to the wind speed (U) increasing C_d.

Total aerodynamic roughness, z_o, is composed of

$$z_o = z_v + z_w + z_f, \tag{1}$$

where z_v is the viscous smooth flow roughness, or tangential stress, associated with the sea surface (Charnock, 1955),

$$z_v = \alpha \frac{u_*^2}{g}, \tag{2}$$

where α~0.011 (Charnock, 1955; Smith, 1988; Fairall et al.,1996), g is the gravitational acceleration, and u_* is the shear velocity. z_w is the wave aerodynamic roughness, owing to form drag and flow separation due to the presence of waves associated with rough flow (Donelan, 1990; Banner and Pierson, 1998; Reul et al., 2008; Mueller and Veron, 2009). z_f is the aerodynamic roughness due to spray droplets and foam and is often included in z_w or z_v. Though z_o can be a linear summation, C_d is not a linear summation (Edson et al., 2013). z_o and C_d at the 10m (subscript 10) for neutral atmospheric stability (subscript N) are related by

$$C_{dN10} = \frac{\kappa}{ln(^{10}/_{z_o})}, \tag{3}$$

where κ (=0.4) is the von Karman constant. Vickers et al. (2013) found that Eq. 2 generally works well for near-neutral stable observations ignoring sea state. Andreas et al. (2012) suggests that the smooth flow formulation (z_v) works for U<8m/s and Donelan (1990) found that the sea becomes fully rough at 7.5m/s. This implies that z_w becomes important for U>8m/s. Andreas et al. (2012) and Edson et al. (2013) found empirical data fits that are a function of U_{N10} using a modified α in Eq. 2. Golbraikh and Shtemler (2016) developed a z_f relationship related strictly to percentage of open-ocean foam coverage and U. It is important to recognize that roughness is increased by an order of magnitude by the presence of foam as compared with a non-foam water surface.

Shabani et al. (2014) indirectly posed a fundamental question – if C_d increases within the surf zone, how are the surf zone waves different from the open ocean waves? Here an alternative hypothesis is proposed that the surface roughness of foam (z_f) generated by depth-limited wave breaking inside the surfzone also contributes to the increased C_d (Figure 1). Within the surfzone, since surface gravity waves are decaying, the potential influence of the wave form drag (z_w) relative to z_f may be reduced, while at the same time z_f is increasing due to increased foam coverage by breaking waves. Using Golbraikh and Shtemler (2016), a modified C_d relationship is developed for surfzone foam coverage.

2. Field Experiment

Co-located sonic anemometers, temperature, and relative humidity sensors were mounted on six, 6-m high towers and deployed simultaneously on four different sandy beaches within the surfzone and near the high-tide line located along 10 km of shoreline in Monterey Bay, CA. Continuous measurements for four weeks in May-June 2016 were divided into 15 minute blocks for analysis. The analysis for computing momentum fluxes and procedures for quality controlling the data are given in Aubinet et al. (2012), which is similar to that described by Shabani et al. (2014) and Ortiz-Suslow et al. (2014).

A pressure sensor and temperature string was deployed in 10m water seaward of each beach tower. Significant wave height (H_{sig}), average wave period (T_{avg}), and wave set-up were estimated from the pressure observations (Dean and Dalrymple, 1995). The tower position and elevation and beach profile were surveyed with a GPS. The distance between the waterline and tower location including wave set-up was estimated for each stress measurement.

H_{sig} and T_{avg} ranged between 0.3-2m and 6-13s associated with local storm-generated events. U_6 measured at 6m elevation ranged from 0-10m/s, with maxima in the late afternoon reducing to near zero at night. A diurnal cycle is observed that is occasionally modified by larger meso-scale atmospheric storm events. The beach air temperature ranged between 10-20^oC. The water temperature ranged from 12-18^oC. The difference of air and water temperatures is predominantly negative implying the atmosphere behaved as an unstable system. Owing to the limitations of empirical formulations used in comparing results, momentum flux data are filtered to limit the range of atmospheric stabilities (ζ) to $-2<\zeta<0.5$, $U_6>3$m/s, and to onshore wind directions that are between $\pm 40^o$ relative to shore-normal. Atmospheric stability is measured as $\zeta = z/L$, where

$$L = \frac{-u_*^3 T_v}{kg\langle w'\theta_v'\rangle}, \tag{4}$$

where T_v is virtual temperature, w' and θ_v' are the turbulent vertical velocity and turbulent virtual potential temperature perturbations, and < > denotes time average. These limitations reduced the analyzed data to 3031 onshore records, out of which 630 records are represented by the surf zone (discussed below), representing 21% of the total data acquired.

The Monterey Bay nearshore system is composed of a relatively steep (1:10) foreshore beach flattening out to a low-tide surfzone terrace (1:100) continuing with a 1:30 offshore slope (MacMahan et al., 2010). The offshore distance for which c equals U_6, is referred to as the decoupling distance (x_{dc}), inside of which the decreasing speed of shoaling waves may increase drag (Antcil and Dolelan, 1996). For the experiment, x_{dc} equals 220m± 80m (1 standard deviation). Considering the surf width is O(100m), the surf zone represents ~30% of the nearshore region for the experimental wind conditions.

2.1 Footprint Analysis

A basic assumption for computing momentum fluxes is that the measurement environment is homogeneous. The nearshore is a heterogeneous environment. The footprint represents the source location where the measured turbulence originates and is estimated by an empirical model that accounts atmospheric stability conditions (Hsieh et al., 2000). It is important to recognize that turbulence measurements obtained on the beach represent turbulence that originates over the ocean that is advected by the wind. The footprint distance (x) increases with increasing stability, wind speed, and measurement elevation (z) and is represented by a skewed probability density function, f(x,z), as described by

$$f(x,z) = \frac{1}{\kappa^2 x^2} D z_u^P |L|^{1-P} exp\left(\frac{1}{\kappa^2 x} D z_u^P |L|^{1-P}\right), \quad (5)$$

where D=0.28, P=0.59 for unstable conditions, D=0.97, P=1 for near neutral conditions, and D=2.44, P=1.33 for stable conditions (Hsieh et al., 2000). z_u is defined as

$$z_u = z\left(\ln\left({z}/{z_o}\right) - 1 + {z_o}/{z}\right). \tag{6}$$

Researchers typically use the maximum of the f(x,z) to denote the source location. Here, the relative percentage of contribution for the source region, R, is estimated by

$$R = \frac{\int_{x1}^{x2} f(x,z)dx}{\int_{0}^{\infty} f(x,z)dx}, \tag{7}$$

where the particular footprint source region, f(x,z), is defined between two cross-shore locations (x_1 and x_2). The data were sub-divided into two categories: the surf zone and seaward of the surf zone based on f(x,z). Data for a region are only considered when R is greater than 70% for that region. Filtering the data for $-2<\zeta<0.5$ and U>3m/s, eliminated all dry-beach observations. It is recognized that the footprint analysis approach, particularly for a heterogeneous environment, is not absolute, but is first step in evaluating C_d for the surfzone region.

This also highlights the applicability of these results to other beaches. For the surf zone to be the primary turbulent source region, the nearshore waters need to be warmer than the associated air temperatures setting up an unstable atmospheric scenario allowing for a relatively narrow footprint to develop.

3. Results

The uncertainties in using stability functions based on Monin-Obukuv similarity theory for adjusting to the stability-corrected C_{dN10} are well-recognized, resulting in a wide range of

C_d, even over homogeneous terrains (Andreas et al., 2012). To avoid these uncertainties, C_{d6} is estimated first directly at z=6m by

$$C_{dz} = \left(\frac{\rho_a \langle u\prime w\prime \rangle}{U_z}\right)^2 = \left(\frac{u_*}{U_z}\right)^2, \qquad (8)$$

where ρ_a is the air density, u' and w' are the turbulent horizontal and vertical velocity perturbations (as measured herein), and < > denotes time average. C_{d6} is O(2x10^{-3}) for the surf zone (Figure 2a). C_{d6} seaward of the surf zone is O(1.5x10^{-3}) (Figure 2a). This suggests that C_{d6} increases over the surf zone. C_{dN10} calculated as a function of U_{N10} using Eq. 8 collapses toward O(1.5x10^{-3}) (Figure 2b). U_{N10} for non-neutral conditions is calculated by

$$U_{N10} = \frac{u_*}{\kappa}\left[ln\frac{10}{z_o} - \psi(\zeta)\right], \qquad (9)$$

where $\Psi(\zeta)$ is the empirical function of the stratification based on stability. Observed open ocean unstable estimates of C_{d10} are larger than C_{dN10} (Vickers et al., 2013). Here it is further related to the footprint analysis, where unstable (stable) conditions result in a smaller (longer) and closer (farther) footprint. Applying Monin-Obukuv similarity theory, $C_{d10}(-\zeta)$ [$C_{d10}(+\zeta)$] values corrected to C_{dN10} are reduced [increased]. In practice, the C_d per source region is dependent upon ζ, which will collapse to a similar C_{dN10}. For the moment, the similarity of C_{dN10} (Figure 2b) is suggested as unique and that the different regions (Figure 2a) potentially represent different mechanisms for modifying C_d.

4. Surfzone foam coverage drag coefficient model

Golbraikh and Shtemler (2016) developed an empirical model for C_d as function of U and foam coverage, δ_f. C_d linearly increases with fractional foam coverage owing to white-capping until saturated foam coverage. Holthuijsen et al. (2012) suggests z_o of foam is related to the characteristic size of the foam bubbles. The sea foam bubble roughness (*k*) is 0.1-2mm (Soloviev and Lukas, 2006) resulting in a surprisingly similar z_o between 0.1-2mm (Powell et al., 2003). The correlation between aerodynamic and geometric roughness is believed related to the idea that the foam is moving in high wind (Golbraickh and Shtemler, 2016). For the surf zone, the foam is assumed not to be moving, as the foam is generated by a wave roller of a self-similar bore and is left behind as the bore moves forward.

Golbraikh and Shtemler (2016) suggest z_o averaged over the sea surface, S, is described as

$$z_o = \frac{S-S_f}{S} z_{ff} + \frac{S_f}{S} z_f = \left(1-\delta_f\right) z_{ff} + \delta_f z_f, \qquad (10)$$

where $S=S_{ff}+S_f$, where S_{ff} is the foam-free surface and S_f is the foam surface, z_{ff} is the foam-free aerodynamic roughness, z_f is the foam-covered aerodynamic roughness, and $\delta_f = S_f/S$ is the fractional foam coverage. For the open ocean, Holthuijsen et al. (2012) developed a δ_f approximation as function of a U_{10}. For the surf zone, δ_f is approximated for depth-limited wave breaking as given by Sinnett and Feddersen (2016)

$$\delta_f = \frac{m\langle\varepsilon_r\rangle}{\rho(gh)^{3/2}}, \qquad (11)$$

where m≅400 and is a fit parameter, $\langle\varepsilon_r\rangle$ is the wave roller dissipation and *h* is the water depth (Battjes, 1975; Feddersen, 2012a,b). The roller dissipation is given by

$$\langle\varepsilon_r\rangle = \frac{2gE_r sin\beta}{c}, \qquad (12)$$

where E_r is the roller energy density and the slope of the roller surface, $\sin\beta=0.1$ (Deigaard, 1993; Duncan, 2001). $\langle\varepsilon_r\rangle$ is estimated from the one-dimensional wave and roller transformation models (Thornton and Guza, 1983; Ruessink et al., 2001) for normally-incident, narrow-banded waves. The roller energy model is defined as

$$\frac{d}{dx}\left(EC_g + 2E_r c\right) = -\langle\varepsilon_r\rangle, \tag{13}$$

where E is the wave energy density, $E = \frac{1}{8}\rho g H_{sig}^2$, C_g is the group velocity, and x is the cross-shore coordinate frame. The Sinnet and Feddersen (2016) surfzone foam coverage model is similar to the breaking wave intensity model as measured by whiteness (as an indication of foam) in video images by Aarninkhof and Ruessink (2004), who also finds the breaking intensity is related to the roller energy dissipation. Examples of the wave height and δ_f are provided in Figure 3a,b for the experiment conditions.

For Monterey beach, δ_f averaged over the surfzone from $H_{sig}(max)$ to the beach is estimated for a range of wave heights and wave periods resulting in a δ_f of 0.35-0.55 (Figure 3a). The foam roughness is defined as

$$z_f \approx \delta_f k \approx \delta_f \frac{k}{3}, \tag{14}$$

where k is the geometric roughness of foam. Applying constant $z_{ff}=2\text{x}10^{-4}$m (Charnock, 1955) and $z_f=2\text{x}10^{-3}$m (Soloviev and Lukas, 2006), the resulting C_{dN10} is O(2 x10^{-3}) (Figure 3b). The open-ocean estimate of z_f being similar to k is most likely an over estimate in the surfzone owing to the foam not moving. Reducing z_f by ~k/3 as suggested by land relationships by Neild et al. (2013) results in a C_{dN10} O(1.5 x10^{-3}) (Figure 3c) similar to the observations (Figure 2b).

The foam-free z_{ff} empirical relationship can be described as a function of wave age, c/u_*, in the open ocean to account for wave form (Drennan et al., 2003),

$$z_{ff} = \frac{H_{sig}}{4} 13.4 \left(\frac{u_*}{c}\right)^{3.4} . \tag{15}$$

with the concept that wave age represents a measure of wave height, and therefore roughness, in generation region. Eqs. 2, 10, 14, and 15 are applied across the shoaling region and surf zone to evaluate the relative contributions of z_o and C_{dN10} (Figure 4c,d). z_{ff} (Eq. 15) increases within the surf zone owing to decreasing c, while H_{sig} is decreasing (Figure 4a). It is also suggested that z_{ff} should decrease in the surf zone, as the waves are decreasing in amplitude which should reduce the form drag. For low winds within the surf zone, z_o and C_{dN10} appear to be governed more by foam, Eq. 14 (Figure 4c,d). As the winds increases, z_{ff} (Eq. 15) unrealistically grows (Figure 5a,b), because c remains a depth-limited constant but u* continues to increase with increasing U. This questions the validity of Eq. 15 parameterized using wave age within the surf zone, particularly for faster wind cases. Using Eq. 2 (*Charnock formulation*) for z_{ff} and z_f ~k/3 in Eq. 10 (black line in Figure 5a,b) results in similar observed surfzone C_{dN10} estimates (black dots in Figure 5a,b). This suggests that summation of Charnock formulation Eq. 2 for z_{ff} and the modified foam model, Eq. 14, in Eq. 10 provides a reasonable estimate of the aerodynamic roughness and corresponding drag coefficient for the surf zone.

Summary & Conclusion

The coupled dynamical relationship between wind and waves in the nearshore region differs from the open ocean. Unlike the open ocean, where surface foam increases as a function of wind speed and concomitant wave height, the wave heights decay while the foam generation increases within the surf zone. This suggests that aerodynamic roughness, z_o, associated with form drag decreases in the surf zone, while surface foam stress increases. Modifying a z_o foam model for the open ocean to a surfzone foam model results in predicted values similar to observed surfzone C_d.

Acknowledgements: This work was supported as part of the ONR Coastal Land Air Sea Interaction (CLASI) pilot experiment. I appreciate the many fruitful conversations with Ed Thornton, Tim Stanton, and Mara Orescanin. Appreciation is extended to the NPS CLASI field team (Jessica Koscinski, Darin Keeter, Paul Jessen, Keith Wyckoff, Mathias Roth, Tucker Freismuth) and CLASI collaborators (*UM:* Brian Haus, Dave Ortiz-Suslow, Hans Graber, Neil Williams; *NPS:* Qing Wang, Dick Lind, and Ryan Yamaguchi; and *NRL:* Jim Doyle, David Flagg). Greg Sinnett provided useful feedback for his model. I thank Falk Feddersen, Baylor Fox-Kemper, and an anonymous reviewer for improving the manuscript clarity.

References:

Andreas, E. L, L. Mahrt, and D. Vickers, 2012: A new drag relation for aerodynamically rough flow over the ocean. J. Atmos. Sci., 69, 2520–2537.

Aarninkhof, S.G.J. and B. G. Ruessink, 2004: Video observations and model predictions of depth-induced wave dissipation IEEE Transactions on Geoscience and Remote Sensing, 42, 11, 10.1109/TGRS.2004.835349.

Anctil, F., and M. A. Donelan, 1996: Air–water momentum flux observations over shoaling waves. J. Phys. Oceanogr., 26, 1344–1353.

Aubinet, M., T. Vesala, D. Papale (Eds.), 2012. Eddy Covariance: A Practical Guide to Measurement and Data Analysis. Springer Atmospheric Sciences, Springer Verlag, 438 pp.

Banner, M. L., and W. L. Peirson, 1998: Tangential stress beneath wind-driven air-water interfaces. J. Fluid Mech., 364, 115–145.

Battjes, J., 1975: Modeling of turbulence in the surfzone. In: Proc. Symposium Modeling Techniques. ASCE, pp. 1050–1061.

Charnock, H., 1955: Wind stress on a water surface. Quart. J. Roy. Meteor. Soc., 81, 639–640.

Dean, R.G. and R.A. Dalrymple, 1995: Water Wave Mechanics for Engineers and Scientists, Prentice-Hall, New Jersey.

Deigaard, R., 1993: A note on the three-dimensional shear stress distribution in a surfzone. Coast. Eng. 20, 157–171.

Donelan, M. A., 1990: Air–sea interaction. The Sea, B. LeMehaute and D. M. Hanes, Eds., Ocean Engineering Science, Vol. 9,Wiley and Sons, 239–292.

Drennan, W. M., H. C. Graber, D. Hauser, and C. Quentin, 2003: On the wave age dependence of wind stress over pure wind seas. J. Geophys. Res., 108, 8062, doi:10.1029/2000JC000715.

Duncan J. H., 2001: Spilling breakers. Annu. Rev. Fluid Mech. 33, 519–47

Edson, J.B., Jampana, V., Weller, R.A., Bigorre, S.P., Plueddemann, A.J., Fairall, C.W., Miller, S.D., Mahrt, L., Vickers, D., Hersbach, H., 2013: On the exchange ofmomentum over the open ocean. J. Phys. Oceanogr. 43, 1589–1610.

Fairall, C. W., E. F. Bradley, D. P. Rogers, J. B. Edson, and G. S. Young, 1996: Bulk parameterization of air–sea fluxes for TOGA COARE. J. Geophys. Res., 101, 3747–3764.

Feddersen, F., 2012a: Scaling surfzone dissipation. Geophys. Res. Lett. 39, L18613.

Feddersen, F., 2012b: Observations of the surfzone turbulent dissipation rate. J. Phys. Oceanogr. 42, 386–399.http://dx.doi.org/10.1175/JPO-D-11-082.1.

Golbraikh, E. and Y. M. Shtemler, 2016: Foam input into the drag coefficient in hurricane conditions, Dynamics of Atmospheres and Oceans, 73,1-9 doi: 10.1016/j.dynatmoce.2015.10.005

Holthuijsen, L.H., Powell, M.D., Pietrzak, J.D., 2012: Wind and waves in extreme hurricanes. J. Geophys. Res. 117, C09003–C9011.

Hsieh C.I., Katul G., Chi T., 2000: An approximate analytical model for footprint estimation of scalar fluxes in thermally stratified atmospheric flows. Advances in Water Resources 23: 765-772. - doi: 10.1016/S0309-1708(99)00042-1

Hsu, S.A., 1970: The shear stress of sea breeze on a swash zone. Proceedings of the 12th International Coastal Engineering Conference, ASCE, 243-255.

MacMahan J.H., Brown J.W., Brown J.A., Thornton E.B., Reniers A.J.H.M., Stanton T.P., Gallagher E.L., Morison J., Austin M.J., Scott T.M., Senechal N., 2010: Mean lagrangian flow behavior on an open coast rip channeled beach: a new perspective. Mar Geol 268:1–15. doi:10.1016/j.margeo.2009.09.011

Mueller, J. A., and F. Veron, 2009: Nonlinear formulation of the bulk surface stress over breaking waves: Feedback mechanisms from air-flow separation. Bound.-Layer Meteor., 130, 117–134.

Nield, J. M., et al., 2014: Estimating aerodynamic roughness over complex surface terrain, J. Geophys. Res. Atmos., 118, 12,948–12,961, doi:10.1002/2013JD020632.

Ortiz-Suslow, D. G., B. K. Haus, N. J. Williams, N. J. M. Laxague, A. J. H. M. Reniers, and H. C. Graber, 2015: The spatial-temporal variability of air-sea momentum fluxes observed at a tidal inlet, J. Geophys. Res. Oceans, 120, 660–676, doi:10.1002/2014JC010412.

Powell, M. D., 2008: High wind drag coefficient and sea surface roughness in shallow water. NOAA/AOML Hurricane Research Division Final Rep. to the Joint Hurricane Testbed, 24 pp. http://www.nhc.noaa.gov/jht/07- 09reports/final_Powell_JHT08.pdf.

Powell, M.D., Vickery, P.J., Reinhold, T.A., 2003: Reduced drag coefficient for high wind speeds in tropical cyclones. Nature 422, 279–283.

Reul, N., Branger, H., Giovanangeli, J.-P., 2008: Air flow structure over short-gravity breaking waves. Bound. Layer Meteorol. 126, 477–505.

Ruessink, B.G., Miles, J.R., Feddersen, F., Guza, R.T., Elgar, S., 2001: Modeling the alongshore current on barred beaches. J. Geophys. Res. 106, 22,451–22,463. 10.1016/j.mio.2016.07.001

Shabani, B., A. V. Babanin, and T. E. Baldock, 2016: Observations of the directional distribution of the wind energy input function over swell waves, J. Geophys. Res. Oceans, 121, 1174–1193, doi:10.1002/2015JC011225.

Shabani, B., P. Nielsen, and T. Baldock, 2014: Direct measurements of wind stress over the surf zone, J. Geophys. Res. Oceans, 119, 2949–2973, doi:10.1002/2013JC009585.

Sinnett, G., and F. Feddersen, 2016: Observations and parameterizations of surfzone Albedo, Methods in Oceanography 17 (2016) 319–334

Smith, S. D., and E. G. Banke, 1975: Variation of the sea surface drag coefficient with wind speed, Q. J. R. Meteorol. Soc., 101, 665–673, doi:10.1002/qj.49710142920.

Soloviev, A., Lukas, R., 2006: The Near-Surface Layer of the Ocean: Structure, Dynamics and Applications. Springer, Dordrecht, Netherlands.

Thornton, E.B., Guza, R.T., 1983: Transformation of wave height distribution. J. Geophys. Res. 88 (C10), 5925–5938.

Vickers, D., L. Mahrt, and E.L. Andreas, 2013: Estimates of the 10-m neutral sea surface drag coefficient from aircraft eddy-covariance measurements, J. Physical Oceanography, 2, doi: 10.1175/JPO-D-12-0101.1

Vugts, H.F. and F. Cannemeijer, 1981: Measurements of drag coefficients and roughness length at the sea-beach interface. J. of Applied Meteorology, 20(4),335-340.

Zachry, B. C., J. L. Schroeder, A. B. Kennedy, J. J. Westerink, C. W. Letchford, and M. E. Hope, 2013: A case study of nearshore drag coefficient behavior during Hurricane Ike (2008), J. Appl. Meteorol. Climatol., 52, 2139–2146.

Figure 1. Picture of the 6-m tall, momentum flux tower deployed on the beach in Monterey, CA highlighting the foam surface coverage and texture within the surf zone in the background. Sonic anemometers were collocated with temperature-humidity sensors located on top of the tower, solar panels were located in the middle, and the data acquisition system is located in the white box. Towers were deployed at the high-tide line, where the tower base was approximately 1.2m above mean sea level.

Figure 2. a) C_{d6} as function of U_6 and **b)** C_{dN10} as a function of U_{N10} for R>70% (Eq. 7) for beyond the surf zone (black squares) and the surf zone (gray triangles). Error bars represent 95% confidence intervals. Colored dots in the center of the symbols represent number of points per bin as described by colorscale to the right.

Figure 3. **a)** Average surfzone foam coverage, δ_f (Eq. 11), **b)** C_{dN10} for z_{ff}=2x10^{-4}m and z_f =2x10^{-3}m, and **c)** C_{dN10} for z_{ff}=2x10^{-4}m and z_f =(2x10^{-3})/3 m, as function of wave height and wave period. Colorscales plotted on top for δ_f and $C_{dN10.}$

Figure 4. The cross-shore distribution of **a)** wave height, **b)** fractional foam coverage, **c)** aerodynamic roughness, and **d)** drag coefficient using a H_{sig}=1.4m, T_{avg}=8s, and u_*=0.2 (U~8m/s), which are representative conditions for the experiment, and a measured beach profile. ff is foam-free (black line, Eq. 15), f is foam (black dashed line, z_f ~*k*/3, Eq. 14), and o is total (gray line, Eq. 10 using Eq. 2 and Eq. 14).

5. a) Neutral, 10m, drag coefficient, C_{dN10} and **b)** aerodynamic roughness, z, for *Charnock formulation*, Eq. 2 (ff, gray line), *wave age formulation*, Eq. 15 (ff, gray dashed line), *surfzone foam formulation*, Eq. 14 (f, black dashed line), and the *Charnock plus surfzone foam formulation*, Eq. 10 (black line), as function of U_{N10}. ff is foam-free (Eq 2. or Eq. 15), f is foam (Eq. 14), and o is total (Eq. 10). Gray triangles with error bars shown in **a)** are measured surfzone C_{dN10} estimates.

Figure 1. Picture of the 6-m tall, momentum flux tower deployed on the beach in Monterey, CA highlighting the foam surface coverage and texture within the surf zone in the background. Sonic anemometers were collocated with temperature-humidity sensors located on top of the tower, solar panels were located in the middle, and the data acquisition system is located in the white box. Towers were deployed at the high-tide line, where the tower base was approximately 1.2m above mean sea level.

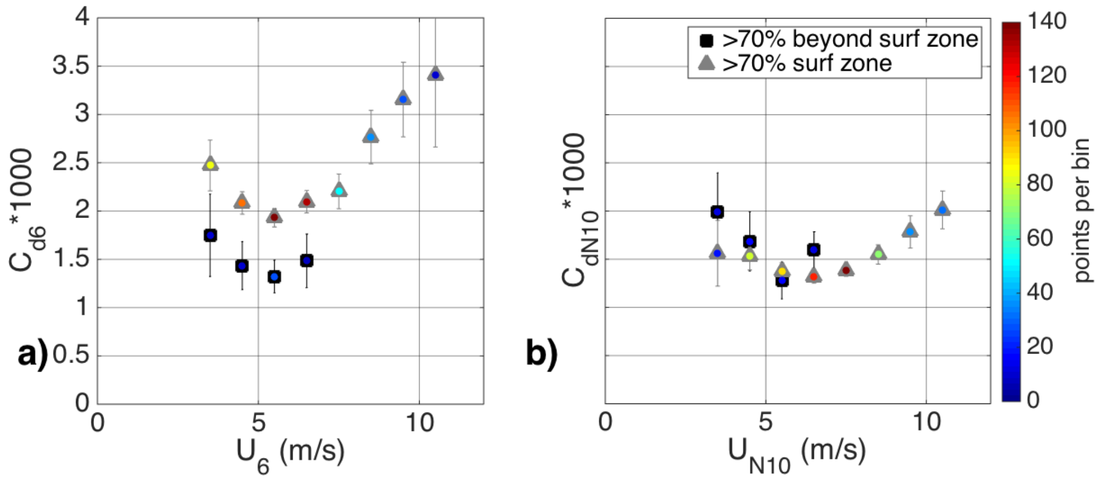

Figure 2. a) C_{d6} as function of U_6 and **b)** C_{dN10} as a function of U_{N10} for R> 70% (Eq. 7) for beyond the surf zone (black squares) and the surf zone (gray triangles). Error bars represent 95% confidence intervals. Colored dots in the center of the symbols represent number of points per bin as described by colorscale to the right.

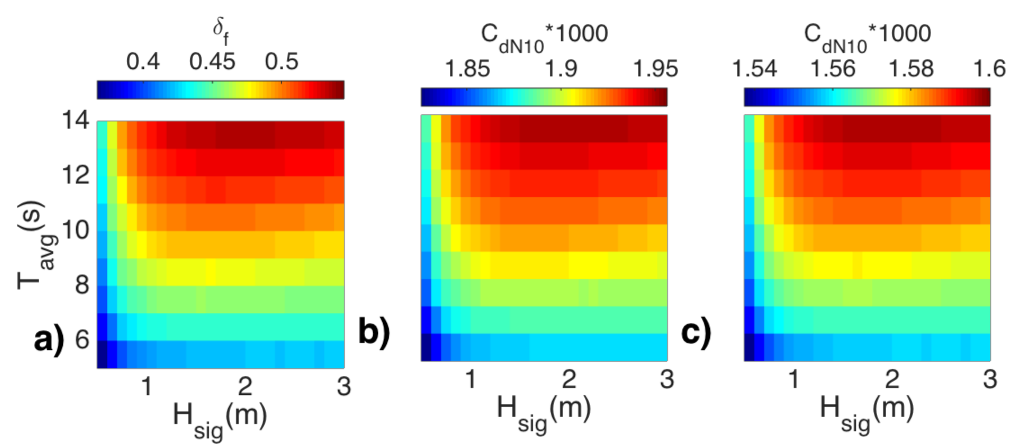

Figure 3. **a)** Average surfzone foam coverage, δ_f (Eq. 11), **b)** C_{dN10} for z_{ff}=2x10^{-4}m and z_f =2x10^{-3}m, and **c)** C_{dN10} for z_{ff}=2x10^{-4}m and z_f =(2x10^{-3})/3 m, as function of wave height and wave period. Colorscales plotted on top for δ_f and C_{dN10}.

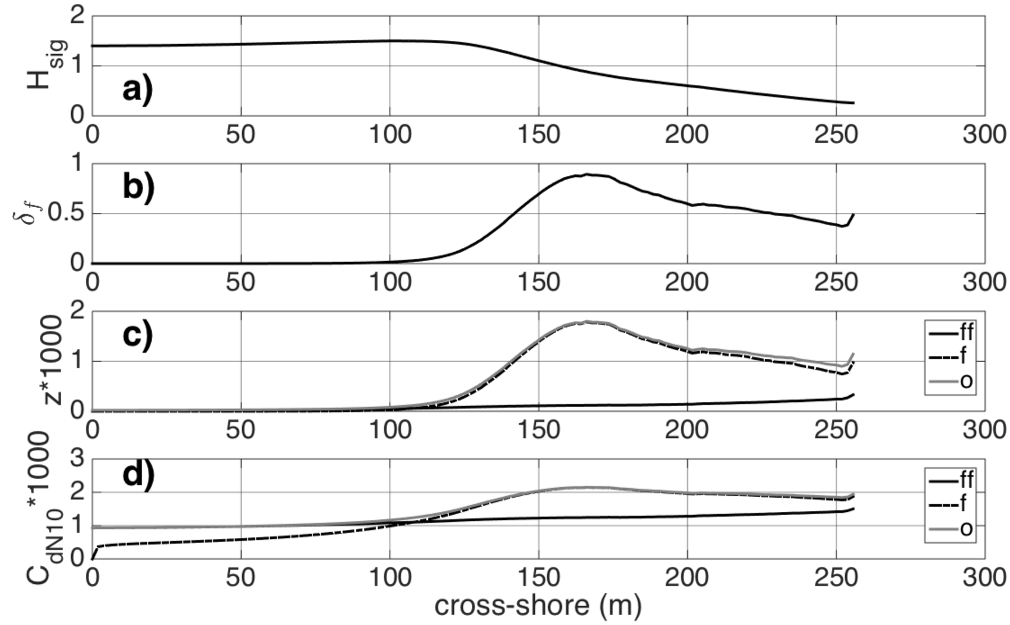

Figure 4. The cross-shore distribution of **a)** wave height, **b)** fractional foam coverage, **c)** aerodynamic roughness, and **d)** drag coefficient using a H_{sig}=1.4m, T_{avg}=8s, and u_*=0.2 (U~8m/s), which are representative conditions for the experiment, and a measured beach profile. ff is foam-free (black line, Eq. 15), f is foam (black dashed line, z_f ~k/3, Eq. 14), and o is total (gray line, Eq. 10 using Eq. 2 and Eq. 14).

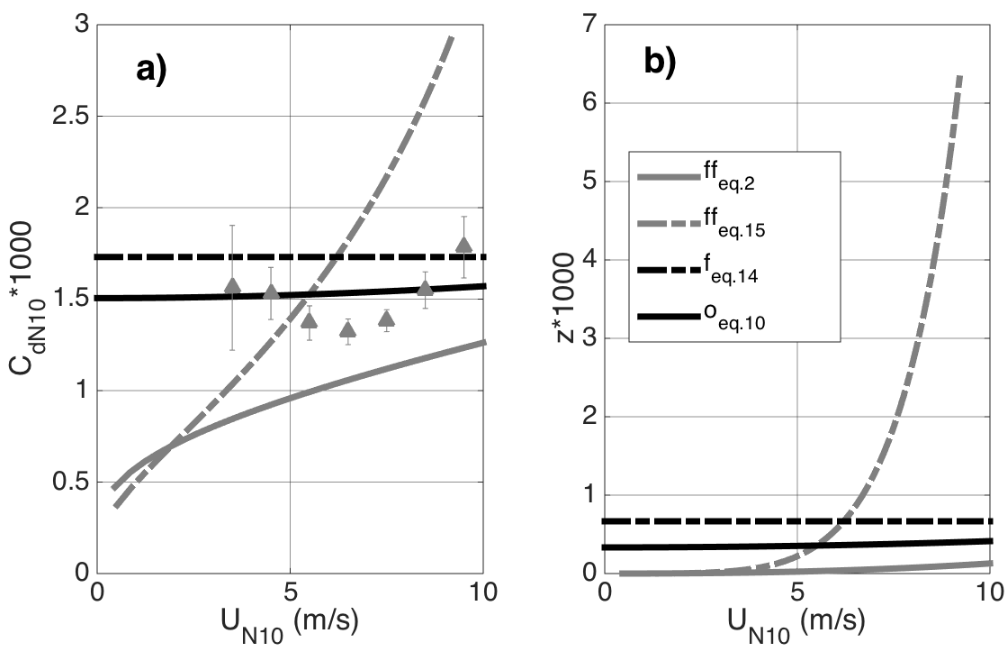

5. a) Neutral, 10m, drag coefficient, C_{dN10} and **b)** aerodynamic roughness, z, for *Charnock formulation*, Eq. 2 (ff, gray line), *wave age formulation*, Eq. 15 (ff, gray dashed line), *surfzone foam formulation*, Eq. 14 (f, black dashed line), and the *Charnock plus surfzone foam formulation*, Eq. 10 (black line), as function of U_{N10}. ff is foam-free (Eq 2. or Eq. 15), f is foam (Eq. 14), and o is total (Eq. 10). Gray triangles with error bars shown in **a)** are measured surfzone C_{dN10} estimates.